Optical Nanoantennas with Tunable Radiation Patterns

Munarriz, J.; Malyshev, A. V.; Malyshev, V. A.; Knoester, J.

Published in:
Nano Letters

DOI:
10.1021/nl303815a

Publication date:
2013

NANO LETTERS

Letter

pubs.acs.org/NanoLett

Optical Nanoantennas with Tunable Radiation Patterns

J. Munárriz,*[,†,‡] A. V. Malyshev,[†,§] V. A. Malyshev,[‡] and J. Knoester[‡]

[†]GISC, Departamento de Física de Materiales, Universidad Complutense, E-28040 Madrid, Spain

[‡]Centre for Theoretical Physics and Zernike Institute for Advanced Materials, University of Groningen, Nijenborgh 4, 9747 AG Groningen, The Netherlands

[§]Ioffe Physical-Technical Institute, St-Petersburg, Russia

ABSTRACT: We address new optical nanoantenna systems with tunable highly directional radiation patterns. The antenna comprises a regular linear array of metal nanoparticles in the proximity of an interface with high dielectric contrast. We show that the radiation pattern of the system can be controlled by changing parameters of the excitation, such as the polarization and/or incidence angles. In the case of excitation under the total reflection condition, the system operates as a nanoscopic source of radiation, converting the macroscopic incident plane wavefront into a narrow beam of light with adjustable characteristics. We derive also simple analytical formulas which give an excellent description of the radiation pattern and provide a useful tool for analysis and antenna design.

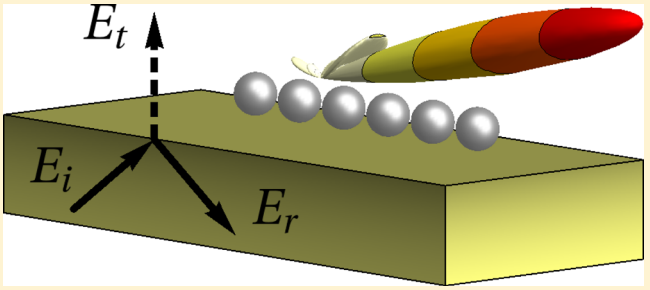

KEYWORDS: *metallic nanoparticle arrays, optical nanoantennas, directional emission, phased array emitters, plasmonics, nanosensing*

Radio and microwave antennas operate as receivers or emitters of electromagnetic radiation within the corresponding wavelength ranges. The size of these devices is typically on the order of the wavelength, which enables one to convert the freely propagating electromagnetic energy into a localized excitation of the antenna and vice versa. Fabricating an optical antenna requires technology of producing objects with subwavelength size, down to several tens of nanometers, which is now possible with modern methods of nanotechnology.[1−6]

Recently, plasmonic antennas, operating in the visible range of the spectrum, have received a great deal of attention.[7−9] Among others, resonator,[10] bow-tie,[11,12] Yagi-Uda,[13] graded,[14,15] cross resonant,[16] core−shell[17] and nanorod[18] configurations have been investigated. Nonlinear plasmonics,[19] nanoscale spectroscopy[20] with optical antennas, and nano-antenna-enhanced gas sensing[21] have also been discussed.

Usually, plasmonic antennas comprise arrays of metallic nanoparticles or nanowires, which convert propagating optical signals into surface plasmon modes or vice versa. One of the challenging tasks here is the antenna excitation. Several schemes have been proposed, ranging from excitation by an adjacent point emitter (such as a single molecule or quantum dot),[18] which requires a very high precision of positioning of the point source, to the excitation by a beam of an electron microscope.[13] Other important and challenging aspects are the design and control of the radiation patterns of such antennas.[13,18] In this paper both issues are addressed theoretically. We consider an antenna system, consisting of a regular linear array of metal nanospheres located close to the interface of two materials with high dielectric contrast. It is shown that the radiation pattern of such a system can be controlled and tuned in a variety of ways, in particular, by changing the angles of incidence and polarization of the excitation beam. We propose to illuminate the system by evanescent waves, which is advantageous from the viewpoint of separation of the excitation from the antenna signal. We show that the radiation pattern of the considered antenna is strongly directional and highly sensitive to the excitation parameters, which can be explained by the interference between the field created by the nanoparticle electric dipoles and their images induced by the interface.

The outline of the paper is as follows. In the next section, we describe the plasmonic antenna system as well as theoretical methods to treat its response. Then, we present results of the numerical calculations of the antenna radiation patterns followed by an approximate analytical treatment which provides insight into the physics of the predicted effects. Finally, we summarize our results and comment on their possible usage and further development.

Model and Formalism. Our model system comprises an array of nanoparticles in close proximity to the interface of two dielectrics with permittivities ε_1 and $\varepsilon_2 > \varepsilon_1$ (see Figure 1). The array is a linear chain of N equally spaced identical metal spheres with radii a and center-to-center distances d, which are embedded in a dielectric with permittivity ε_1 at a center-to-interface distance h (the chain is parallel to the interface). The ratios $a/d \leq 1/3$ and $a/h \leq 1/3$ are chosen in such a way that the point dipole approximation for the interactions between different particles can be used. The former condition on the

Received: October 10, 2012
Revised: January 18, 2013
Published: January 22, 2013

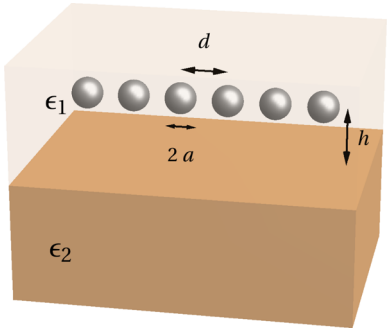

Figure 1. System schematics: a regular linear array of identical spherical metal nanoparticles located parallel to the interface between two dielectrics with permittivities ε_1 and ε_2 ($\varepsilon_1 < \varepsilon_2$), a is the nanosphere radius, d is the center-to-center, and h is the center-to-interface distance.

sphere radius and the center-to-center distance was discussed in refs 22 and 23. The latter relationship is analogous; to verify its validity we compared results obtained within the point dipole approximation with those calculated using the boundary-elements method,[24] which were in good agreement. Because of this we use simpler and numerically less demanding methods based on the point-dipole approximation henceforth.

The nanospheres are characterized by their polarizabilities $\alpha(\omega)$, where ω is the frequency of the incident field. The polarizability of small particles (compared with the wavelength) in a homogeneous environment can be described retaining the first two correction terms:[25,26]

$$\frac{1}{\alpha(\omega)} = \frac{1}{\alpha^{(0)}(\omega)} - \frac{k_1^2}{a} - i\frac{2}{3}k_1^3 \tag{1}$$

where $\alpha^{(0)}(\omega)$ is the bare quasi-static polarizability of the sphere, $k_1 = (\omega/c)(\varepsilon_1{}^{1/2})$ is the wave vector of light in the medium embedding the spheres, and c is the speed of light in vacuum. The term quadratic in k_1 describes the depolarization shift of the plasmon resonance, while the cubic one accounts for the radiative damping.[26] Dielectric or metallic surfaces in the proximity of a sphere can also modify its polarizability (see below). Within the quasi-static approximation, the bare polarizability $\alpha^{(0)}$ is expressed in terms of the frequency dependent dielectric constant of the bulk nanoparticle material, $\varepsilon_M(\omega)$, and that of the embedding dielectric:[27,28]

$$\alpha^{(0)}(\omega) = a^3\frac{\varepsilon_M(\omega) - \varepsilon_1}{\varepsilon_M(\omega) + 2\varepsilon_1} \tag{2}$$

In the point dipole approximation, the induced dipole moment of the n-th sphere p_n can be obtained by solving the following set of equations:

$$\mathbf{p}_n = \varepsilon_1\alpha(\omega)[\mathbf{E}_0(\mathbf{r}_n) + \sum_m \hat{\mathbf{G}}(\mathbf{r}_n, \mathbf{r}_m)\mathbf{p}_m] \tag{3}$$

where m and n run from 1 to N, $\mathbf{r}_n$ is the position vector of the center of the n-th sphere, $\mathbf{E}_0(\mathbf{r}_n)$ is the total external electric field (either the refracted one, if illuminated from the ε_2 side, or a superposition of the direct excitation and that reflected from the interface, if excited from the ε_1 side), and $\hat{\mathbf{G}}(\mathbf{r},\mathbf{r}')$ is the Green's tensor of the total secondary dipole field:

$$\hat{\mathbf{G}}(\mathbf{r}, \mathbf{r}') = \begin{cases} \hat{\mathbf{G}}_0(\mathbf{r}, \mathbf{r}') + \hat{\mathbf{G}}_r(\mathbf{r}, \mathbf{r}') & \mathbf{r} \neq \mathbf{r}' \\ \hat{\mathbf{G}}_r(\mathbf{r}, \mathbf{r}') & \mathbf{r} = \mathbf{r}' \end{cases} \tag{4}$$

Here, $\hat{\mathbf{G}}_0(\mathbf{r},\mathbf{r}')$ is the Green's tensor in a homogeneous medium giving the electric field created at point $\mathbf{r}$ by a unit dipole located at $\mathbf{r}'$:[29]

$$\hat{\mathbf{G}}_0(\mathbf{r}, \mathbf{r}') = \frac{1}{\varepsilon_1}(\nabla\nabla + k_1^2\mathbf{1})\frac{\exp(ik_1|\mathbf{r} - \mathbf{r}'|)}{|\mathbf{r} - \mathbf{r}'|} \tag{5}$$

where $\nabla\nabla$ is the dyadic product of the nabla operators and $\mathbf{1}$ is the unit dyadic. $\hat{\mathbf{G}}_r(\mathbf{r},\mathbf{r}')$ is the Greens' tensor of the reflected dipole field, which describes the interaction between nanoparticles mediated by the interface. This tensor can be calculated numerically using the Sommerfeld integrals formalism which has been extensively studied and widely used throughout the literature.[30−32] The self-interaction term $\hat{\mathbf{G}}(\mathbf{r}_n,\mathbf{r}_n)$ corrects the polarizability, eq 1, for the presence of the interface and guarantees, in particular, the correct energy balance.

For any given external field $\mathbf{E}_0(\mathbf{r})$, the system of equations in eq 3 is linear in $\mathbf{p}_n$, and the induced dipole moments can be computed by standard numerical methods. Once they are obtained, it is straightforward to calculate the total electric field at an arbitrary point $\mathbf{r}$ (located outside the volumes of the spheres):

$$\mathbf{E}(\mathbf{r}) = \mathbf{E}_0(\mathbf{r}) + \sum_m \hat{\mathbf{G}}(\mathbf{r}, \mathbf{r}_m)\mathbf{p}_m \tag{6}$$

We are interested in the radiation of the antenna (i.e., in the far-zone component of the scattered field) above the interface. We consider excitations from the ε_2 side (from below) under conditions of total reflection. Then, the incident field $\mathbf{E}_0(\mathbf{r})$ is an evanescent wave in the upper half-space, and its contribution to the total field is negligible if the detection point is sufficiently far from the interface. In this case, the far field is governed by the second term in eq 6. To obtain the antenna radiation pattern, one should calculate the angular dependence of the radiant intensity $U(\theta,\phi)$ on an enclosing sphere centered at the system and having a radius $R \gg \lambda_1$, where $\lambda_1 = 2\pi/k_1$ is the excitation wavelength in the medium. This intensity is given by

$$U(\theta, \phi) \propto R^2|\sum_m \hat{\mathbf{G}}(\mathbf{R}, \mathbf{r}_m)\mathbf{p}_m|^2 \tag{7}$$

As we show below, radiation patterns of the antenna considered here can be highly directional: typically, they have a narrow main lobe and a set of much weaker side lobes. To characterize the directionality of the antenna radiation quantitatively, we use the standard directivity parameter:

$$D = \frac{\max U(\theta, \phi)}{\int_{2\pi} U(\theta, \phi)d\Omega/2\pi} \tag{8}$$

which is the ratio between the maximum radiant intensity and the average one. The integration in eq 8 is performed over the solid angle of 2π (instead of the usual 4π), because we are interested in the radiation in the upper half-space only.

Numerical Results. We calculated the antenna radiation patterns for a linear array of $N = 15$ identical silver nanospheres in proximity to the interface between two media with refractive indices $n_1 = (\varepsilon_1)^{1/2} = 1.5$ (above the interface) and $n_2 = (\varepsilon_2)^{1/2} = 2.1$ (below the interface). Other parameters of the model were chosen as follows: the nanosphere radius $a = 45$ nm, the

dx.doi.org/10.1021/nl303815a | Nano Lett. 2013, 13, 444−450

interparticle separation d = 180 nm, and the array-to-interface distance h = 135 nm. Tabulated data for the permittivity of silver[33] were used to calculate the polarizability of the nanospheres.

We assume that the system is illuminated by a plane wave with the wavelength in vacuum λ_0 = 610 nm, incident from the medium below the interface, while we are interested in the radiation into the upper half space. Let the spherical coordinates of the detection point be (R,θ,ϕ) with $\theta \in [0,\pi/2]$ and $\phi \in [0,2\pi]$ ($\phi = 0$ in the direction of the array), while Θ and Φ are the polar and azimuthal angles of incidence of the incoming plane wave (see Figure 2). To excite the system by an evanescent wave the incidence polar angle Θ should lie within an interval $(\Theta_c,\pi/2)$, where $\Theta_c = \arcsin(n_1/n_2)$ is the angle of the total reflection; for the considered system Θ_c = 45.6°. Finally, we will also distinguish between the s and p polarizations of the excitation.

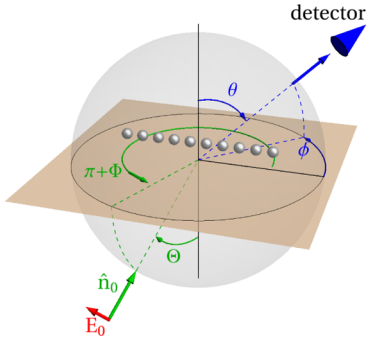

Figure 2. Geometry of the excitation and detection: $\mathbf{E}_0$ is the excitation field, $\hat{\mathbf{n}}_0 = \mathbf{k}_2/k_2$ describes the direction of its incidence, and $0 \le \Theta \le \pi/2$ and $-\pi/2 \le \Phi \le \pi/2$ are the polar and azimuthal angles of incidence. The blue cone represents the detector whose angular coordinates are θ and ϕ.

Figure 3 shows radiation patterns calculated for the s-polarized excitation incident at a polar angle Θ = 50° > Θ_c and different azimuthal angles: Φ = 0°, 30°, 45°, 60°, 75°, and 90°. The figure demonstrates that in all cases the radiation is highly directional; the directivity D is given in the white rectangle in each plot. The interference between the fields scattered by the nanoparticles is constructive only within a relatively narrow solid angle, giving rise to the formation of the main lobe of the pattern. As we show below, its shape can be obtained analytically. It is clear from the comparison of the incidence geometry (see green arrows in Figure 3) and the position of the main lobe that the latter is formed by the forward scattered light.

As can be seen from Figure 3, the orientation of the main lobe varies smoothly with the azimuthal angle of incidence Φ. Much more pronounced and abrupt changes can occur if the incidence is more oblique. For example, for Θ = 60° the antenna main lobe orientation can be almost reversed by a relatively small change of the azimuthal angle Φ, as shown in the upper panels of Figure 4. In the lower panel of the figure we plotted cross sections of the main lobes for two different excitation conditions, which demonstrate that the predominant scattering switches from the forward to the backward one when the azimuthal angle Φ changes from 30° to 10°. A similar switching effect is observed in the lower optically denser medium too (see Figure 5). Note that the angles of the main radiation lobes are different from the angles of incidence and reflection; therefore, the excitation will not interfere with the signal, which can facilitate measurements.

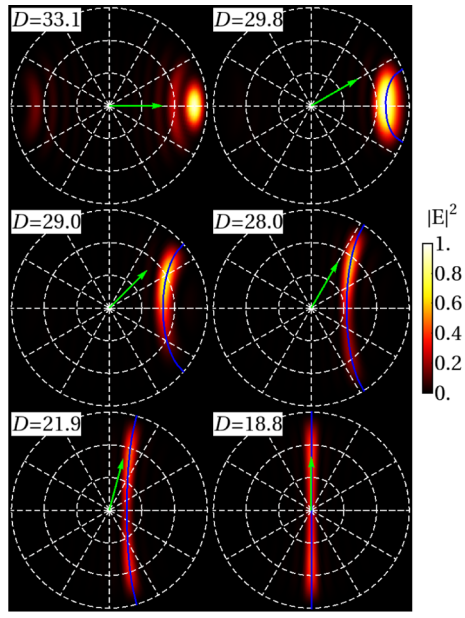

Figure 3. Polar plots of the radiation patterns of the antenna described in the text. The color gives the far-field intensity as a function of the detection angles θ and ϕ. The polar angle θ changes linearly along the radius from 0 to $\pi/2$ (dashed circles are drawn each 30°). The system was excited by an s-polarized plane wave with angles of incidence Θ = 50° and (from left to right) Φ = 0°, 30° (upper row), 45°, 60° (middle row), 75°, 90° (lower row). The excitation propagation direction is represented schematically by the green vector; its end point has the angle coordinates (Θ,Φ). The directivity D of the radiation pattern is given in the white rectangle in each plot. Blue lines represent the main lobe position calculated within the image dipole and stationary phase approximations, as described in the next section (see text for more details).

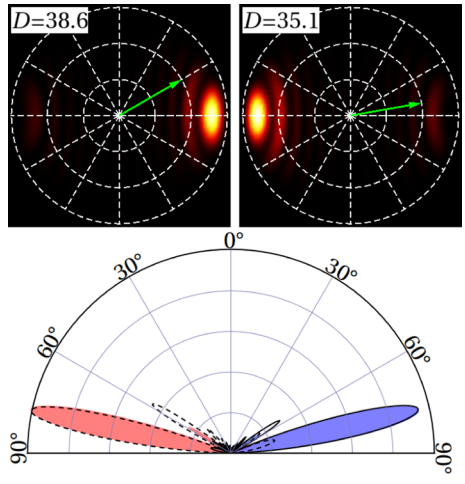

Figure 4. Upper row—same as in Figure 3, but for incidence at Θ = 60° and Φ = 30° (left) and Φ = 10° (right). Switching of the antenna radiation direction is observed when the azimuthal angle Φ changes within a relatively narrow range. The lower plot shows the cross sections of the two radiation patterns computed for ϕ = 0: blue and pink filled areas correspond to Φ = 30° and Φ = 10°, respectively. The black solid and dashed lines represent the same cross sections calculated according to the approximate formula in eq 11.

dx.doi.org/10.1021/nl303815a | Nano Lett. 2013, 13, 444−450

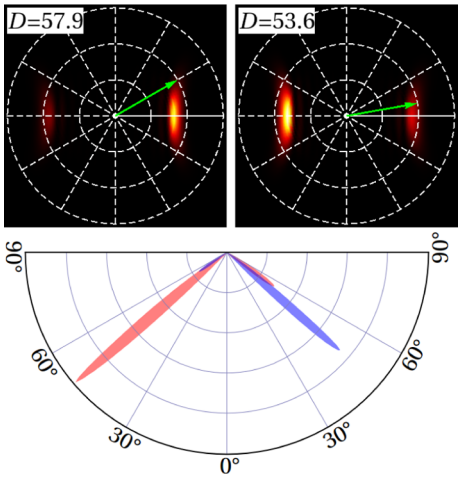

Figure 5. Same as in Figure 4, but for the lower half-space. The polar angle θ is measured from the normal to the interface pointing down.

The power radiated by a dipole in the proximity of a dielectric interface is higher in the optically denser medium. For the considered system about 10% of the total scattered power goes into the upper half-space. The scattered intensity is proportional to the incident one and is limited therefore by the maximum possible dissipated power determined by the melting threshold of the nanoparticles.

Figure 6 shows the dependence of the directivity on the incidence angles Θ and Φ. The switching effect takes place in

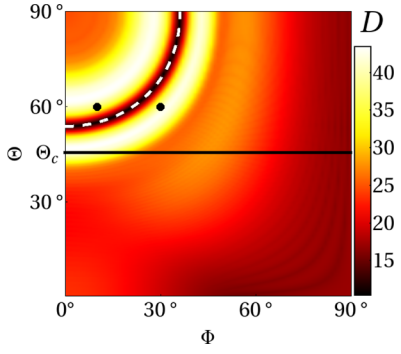

Figure 6. Directivity versus the incidence angles Θ and Φ. The dashed line shows the incidence at which the phase difference between adjacent induced dipoles is π. The dots correspond to the illumination conditions used in Figure 4.

the vicinity of the pronounced dip in the directivity; the directivity is decreased when the phase difference between adjacent induced dipoles is equal to π (see the white dashed line in the figure). In this case their is a mirror symmetry in the far-field pattern with respect to the plane $\theta = \pi/2$ and two identical lobes of forward and backward scattered light coexist. The two neighboring light-colored quarter-circle features are determined by the strong forward *or* backward scattering condition, when the far-field pattern is characterized by a single highly directional lobe. When the dip is crossed, the direction of the main lobe is switched abruptly.

Finally, we address the effect of the polarization of the incoming light on the radiation pattern. The polarization affects the direction of the induced particle dipoles, whose far field interference determines the shape of the pattern. The effect of polarization is expected to be most pronounced for $\Phi = 90°$, because in this case the *s*-polarized light induces dipoles almost parallel to the antenna axis, while the *p*-polarized excitation favors the dipole orientation perpendicular to the axis. We calculated the radiation patterns for the two excitation polarizations in the case of $\Theta = 46°$ and $\Phi = 90°$; the results are shown in Figure 7. The upper panels present the full polar

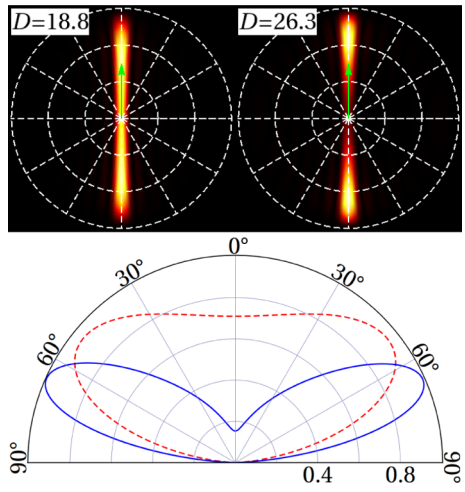

Figure 7. Upper row—radiation patterns for $\Theta = 46° \gtrsim \Theta_c$ and $\Phi = 90°$ for two different polarizations of the excitation: *s* (left panel) and *p* (right panel). The lower plot shows cross sections of the two patterns at $\phi = \pi/2$: red dashed and solid blue lines correspond to *s* and *p*-polarized excitations, respectively.

patterns, while the lower one shows their cross sections for $\phi = \pi/2$. As expected, the most pronounced difference between the two cases is observed in the vicinity of the polar angle $\theta = 0$ where the pattern has a pronounced dip in the case of *p*-polarized excitation while the radiation is strong in the other case.

Thus, the radiation pattern of the system can be adjusted by changing the excitation parameters, such as the geometry of incidence or polarization, which can easily be controlled in the experiment.

Analytical Results and Discussion. In this section we present an approximate analytical approach for the calculation of the antenna radiation pattern, combining the image dipole and stationary phase approximations. Analytical results allow us to gain insight into the physics of the system's response and to understand qualitatively the numerical results obtained in the previous section. Moreover, our simple analytical formulas can be used to solve the inverse problem: engineer the geometry of the system and excitation meeting particular requirements, such as a desired radiation pattern.

The radiation pattern is determined by the intensity of the secondary scattered field in the far zone. If a *single* dipole p is located at $\{0,0,h\}$ (we use Cartesian coordinates for dipole positions for convenience) and $R \gg h$, its radiation reads

$$\mathbf{E}_{\mathrm{d}}(\theta, \phi) \approx \frac{k_1^2[\mathbf{p} - (\mathbf{p}\cdot\mathbf{n})\mathbf{n}]}{\varepsilon_1 R} e^{-ik_1 h\cos\theta} e^{ik_1 R} \quad (9)$$

where n is the unit vector, pointing in the direction of the detection (θ and ϕ are its angular coordinates). Note that the last exponential factor, determined by the overall phase k_1R, is an angle-independent common factor, and therefore it is irrelevant for the field intensity. Being in close proximity to the

dx.doi.org/10.1021/nl303815a | Nano Lett. 2013, 13, 444−450

interface, the dipole induces surface charge density whose electric field contributes to the radiation as well. This secondary reflected field $\mathbf{E}_r$ is given by the Sommerfeld integrals which can be calculated in the far-zone of the upper medium by making use of the stationary phase approximation.[32] The result reads:

$$\mathbf{E}_r(\theta, \phi) = e^{2ik_1 h\cos\theta}[\mathcal{F}_s(\theta)(\mathbf{E}_d(\theta, \phi)\cdot\mathbf{e}_s)\mathbf{e}_s + \mathcal{F}_p(\theta)(\mathbf{E}_d(\theta, \phi)\cdot\mathbf{e}_p)\mathbf{e}_p] \quad (10)$$

where $\mathcal{F}_s(\theta, \phi)$ and $\mathcal{F}_p(\theta, \phi)$ are the Fresnel reflection coefficients for the *s*- and *p*-polarized waves[2] incident from the upper medium onto the interface, $\mathbf{e}_s$ and $\mathbf{e}_p$ are unit vectors of the *s*- and *p*-polarized components of the radiated field: $\mathbf{e}_s = \mathbf{n} \times \mathbf{n}_z/|\mathbf{n} \times \mathbf{n}_z|$ ($\mathbf{n}_z$ being the normal to the interface pointing up) and $\mathbf{e}_p = \mathbf{n} \times \mathbf{e}_s$. As is seen from the comparison of eqs 9 and 10, the secondary field $\mathbf{E}_r$ is equivalent to that produced by an image dipole placed at $\{0, 0, -h\}$ in a homogeneous medium with the dielectric constant ε_1. However, the *s* and *p* components of the reflected field $\mathbf{E}_r$ are renormalized by the corresponding Fresnel reflection coefficients.

The radiation of an array of dipoles is the superposition of their far fields; its intensity angular distribution depends exclusively on the relative phases of the contributing fields (a relatively small shift of the coordinate origin would result in an additional common angular independent, and therefore irrelevant, phase of the field). When such dipoles are arranged in a regular linear chain and $R \gg Nd$, the total secondary far field can be calculated analytically, using the following additional approximations. First, we assume that the phase and orientation of the *n*-th dipole is determined by the phase and polarization of the external field $\mathbf{E}_0(\mathbf{r}_n)$ acting upon it and, second, that all dipoles have the same amplitude. It turns out that, for the considered system, excitation geometries and wavelengths these approximations are reasonable. In this case, the phase difference between two dipoles located at $\{x_1,0,h\}$ and $\{x_2,0,h\}$ is $k_1 n_{21}(x_2 - x_1)\sin\Theta\cos\Phi$ with $n_{21} = n_2/n_1$. On the other hand, the phase difference in the far fields of the two dipoles is $k_1(x_2 - x_1)\sin\theta\cos\phi$. Using all of the above assumptions and the corresponding phase relations, one can sum the fields produced by all dipoles and their images, arriving finally at the following expression for the radiation:

$$\mathbf{E}(\theta, \phi, \Theta, \Phi) = \frac{\sin(\beta N/2)}{\sin(\beta/2)}[\mathbf{E}_d(\theta, \phi) + \mathbf{E}_r(\theta, \phi)] \quad (11)$$

where β is the phase difference of the radiation of two neighboring particles,

$$\beta = k_1 d(\sin\theta\cos\phi - n_{21}\sin\Theta\cos\Phi) \quad (12)$$

In the adopted approximation, the orientation of the induced dipoles is dictated by the polarization of the incident field $\mathbf{E}_0$. If the excitation is *s*-polarized, the dipoles are oriented along $\Phi + \pi/2$, and no field is radiated in this direction. If the detection angle ϕ is not close to $\Phi + \pi/2$, the fields in the square brackets in eq 11 are smooth functions of θ and ϕ. Therefore, it is the fraction of the two sine functions in eq 11 that determines the lobe structure of the radiation pattern (a detailed discussion of this prefactor can be found, for example, in ref 34). This fraction is large when $\beta = 2\pi n$ with an integer *n*, in which case the interference is constructive and the far-field of *N* dipoles is about *N* times larger than that of a single dipole. Hence, the enhancement factor of the radiated intensity over that of a single nanoparticle is on the order of N^2. Strong far-field lobes are formed in the vicinity $\delta\beta \ll 2/N$ of the scattering angles giving solutions to the equation $\beta = 2\pi n$. This vicinity becomes smaller as *N* increases, resulting in the narrowing of the lobes. On the contrary, if θ and ϕ are such that $\beta N = 2\pi n$ where *n* is not a multiple of *N*, the interference is destructive, and the antenna is only weakly radiating in these directions. Essentially, eq 11 gives the far-field of a double chain of identical dipoles and their images.

The lower panel of Figure 4 shows the radiation pattern cross sections calculated numerically, according to eq 7, (blue and pink filled areas correspond to $\Phi = 10°$ and 30°, respectively) and those obtained using the approximate analytical expression in eq 11 (solid and dashed lines). The amplitude of the analytical result was scaled to get the same maximum as the numerical result. The figure demonstrates that the analytical expression gives an excellent description of the main lobes of the patterns. For the chosen polar angle of incidence $\Theta = 60°$, the main lobe almost reverses its direction when the azimuthal angle of incidence changes from $\Phi = 10°$ to $\Phi = 30°$. Below, we provide a simple qualitative explanation of this behavior based on the analysis of our approximate formula.

To understand the underlying physics of the predominant scattering direction switching, we note that the phase β can be rewritten in terms of the projection of the incoming and outgoing wave vectors onto the chain axis: $\beta = (k_{1x} - k_{2x})d$. The interference is constructive when $\beta = 2\pi n$, which can be interpreted as the diffraction condition: $k_{1x} - k_{2x} = 2\pi n/d$, where $2\pi n/d$ are the vectors of the reciprocal lattice with the lattice constant *d*. The latter relationship is the momentum conservation law for a periodic structure where the *k*-vector is conserved to within a vector of the reciprocal lattice.

The constructive interference condition $\beta = 2\pi n$ is the standard diffraction grating equation. However, there is an important aspect. In the considered system, the fact that the lower medium is optically denser than the upper one (i.e., $k_2 > k_1$) plays the key role and results in the appearance of qualitatively new solutions as compared to the traditional diffraction case. As long as $k_{2x} \le k_1$ the condition $\beta = 0$ can be met for $\theta \approx \Theta$ and $\phi \approx \Phi$; that is, the direction of the main lobe is close to that of the incidence resulting in strong "forward" scattering. Moreover, for the range of parameters chosen, $k_1 d < \pi$, and therefore the scattering pattern is always characterized by a single strong lobe.

On the other hand, for $k_{2x} > k_1$, forward scattering is forbidden because it would require a wave vector larger than the one allowed in the upper medium. In this qualitatively new situation, the constructive interference occurs for the outgoing wave vectors which differ from the incoming ones by a vector of the reciprocal lattice. In particular, the condition $\beta = -2\pi$ can be met when k_{1x} and k_{2x} have opposite signs. The latter is the "backward" scattering observed in Figure 4.

Because the switching effect is determined by the underlying momentum translation condition, which is a consequence of the symmetry of the system, it is expected to also hold for different excitation wavelengths and geometrical parameters, for example, for arrays deposited closer to the interface.

Figure 7 demonstrates that the antenna radiation patterns can be controlled also by the polarization of the incident light, which is a parameter that can easily be changed in an experiment. In Figure 7, the polar angle of incidence Θ is only slightly larger than the angle of total reflection while the azimuthal angle $\Phi = \pi/2$ implies incidence normal to the chain

dx.doi.org/10.1021/nl303815a | Nano Lett. 2013, 13, 444−450

axis. Under these conditions, the main lobe of the pattern is determined by the equation $\beta = 0$, having the obvious solution $\phi = \pi/2$. The θ-dependence of the patterns in this case is dictated by the excitation polarization. For the *s*-polarized excitation, all dipoles are oriented along the chain, that is along $\phi = 0$, and the radiation is efficient within a continuous broad range of polar angles θ (see the dashed red line in the lower panel of Figure 7). Contrary to that, when the excitation is *p*-polarized, all dipoles are almost perpendicular to the chain axis and to the interface plane, that is along $\theta = 0$. According to eq 9, a dipole does not radiate in its own direction, which explains the appearance of a pronounced dip around $\theta = 0$ in the radiation pattern (see the blue solid line in the lower panel of Figure 7).

Summary. We addressed radiation patterns of a plasmonic antenna comprising a regular linear chain of identical metal nanospheres in close proximity to an interface between two media with high dielectric contrast. When such a system is illuminated from the higher refractive index side of the interface it can be excited by evanescent waves. In this case the excitation does not mask the useful antenna signal, which is advantageous for measurements and applications. We showed that the radiation pattern and its directivity can be controlled by changing the incidence angles and/or polarization of the excitation. In particular, for some excitation geometries, the antenna pattern is characterized by a very narrow main lobe whose direction can be changed abruptly by a relatively small change of incidence angles.

We have calculated the antenna radiation patterns using the traditional, much more numerically elaborated and accurate, Sommerfeld integrals approach, and a much simpler one, based on the image dipole and the stationary phase approximations. We have shown that, despite the complexity of the system, our analytical expression for the radiation patterns gives an excellent description of the main features of the antenna response. These simple formulas can become a useful tool for solving the inverse problem: engineering a system that has a desired radiation pattern. For example, analyzing the formulas it is possible to figure out the system and excitation geometries giving rise to a particular direction and directionality of the main lobe.

An antenna comprising identical nanoparticles operates within a relatively narrow bandwidth; however, the spectral range can be broadened by using graded plasmonic arrays.[14,15] We note that, although we considered the theoretically simplest case of the chain of nanospheres, our results are expected to be valid for arrays of particles with more complex shapes, such as discs, which can be easier to fabricate. Real-life structures always have fabrication imperfections. It is quite clear that a disorder would lead to some smearing of the features of the far-field pattern. However, the plasmon resonances of metal nanoparticles are broad and a relatively small change of the particle sizes would not affect their polarizability (hence, the induced dipoles) to a large extent. The same can be said about the interaction: being a long-range one it is not very sensitive to small deviations of particle positions. A more detailed quantitative study of disorder effects goes beyond the scope of this Letter.

Similar ideas and approaches can be applied to more complicated nanostructures, such as 2D arrays or metamaterials.[35] The dielectric interface would still play its key role, contributing two important aspects: the dielectric contrast is an additional degree of freedom allowing to control radiation patterns of the nanoscopic sources of light, while excitation by evanescent waves results in the conversion of a macroscopic plane wave into a narrow beam of light with adjustable characteristics and direction. Apart from being an interesting fundamental phenomenon, this opens new possibilities in optical nanodevices design and new opportunities to control the flow of electromagnetic energy at the nanometer scale, in particular, for precisely addressing and exciting nanoscopic objects such as nanostructures, quantum dots, single molecules, and so forth.

AUTHOR INFORMATION

Corresponding Author

*E-mail: j.munarriz@fis.ucm.es.

Notes

The authors declare no competing financial interest.

ACKNOWLEDGMENTS

This work has been supported by MICINN (projects Mosaico and MAT2010-17180 in Spain). J.M. also acknowledges support from the University of Groningen. V.A.M and J.K. acknowledge NanoNextNL, a micro and nanotechnology consortium of the Government of The Netherlands and 130 partners.

REFERENCES

(1) Maier, S. A.; Atwater, H. A. *J. Appl. Phys.* **2005**, *98*, 011101.
(2) Novotny, L.; Hecht, B. *Principles of Nano-Optics*; Cambridge University Press: Cambridge, U.K., 2006.
(3) Maier, S. *Plasmonics: Fundamentals and Applications*; Springer: New York, 2007.
(4) Ozbay, E. *Science* **2006**, *311*, 189−193.
(5) de Waele, R.; Koenderink, A. F.; Polman, A. *Nano Lett.* **2007**, *7*, 2004−2008.
(6) Atwater, H. A.; Polman, A. *Nat. Mater.* **2010**, *9*, 205−213.
(7) Brongersma, M. L. *Nat. Photonics* **2008**, *2*, 270−272.
(8) Bharadwaj, P.; Deutsch, B.; Novotny, L. *Adv. Opt. Photonics* **2009**, *1*, 438−483.
(9) Novotny, L.; van Hulst, N. *Nat. Photonics* **2011**, *5*, 83−90.
(10) Barnard, E. S.; White, J. S.; Chandran, A.; Brongersma, M. L. *Opt. Express* **2008**, *16*, 16529−16537.
(11) Zhang, Z.; Weber-Bargioni, A.; Wu, S. W.; Dhuey, S.; Cabrini, S.; Schuck, P. J. *Nano Lett.* **2009**, *9*, 4505−4509.
(12) Yang, Y.-Y.; Zhang, Y.-L.; Jin, F.; Dong, X.-Z.; Duan, X.-M.; Zhao, Z.-S. *Opt. Commun.* **2011**, *284*, 3474−3478.
(13) Coenen, T.; Vesseur, E. J. R.; Polman, A.; Koenderink, A. F. *Nano Lett.* **2011**, *11*, 3779−3784.
(14) Malyshev, A. V.; Malyshev, V. A.; Knoester, J. *Nano Lett.* **2008**, *8*, 2369−2372.
(15) Pavlov, R. S.; Curto, A. G.; van Hulst, N. F. *Opt. Commun.* **2012**, *285*, 3334−3340.
(16) Biagioni, P.; Huang, J. S.; Duò, L.; Finazzi, M.; Hecht, B. *Phys. Rev. Lett.* **2009**, *102*, 256801.
(17) Bardhan, R.; Grady, N. K.; Ali, T.; Halas, N. J. *ACS Nano* **2010**, *4*, 6169−6179.
(18) Taminiau, T. H.; Stefani, F. D.; van Hulst, N. F. *Nano Lett.* **2011**, *11*, 1020−1024.
(19) Palomba, S.; Danckwerts, M.; Novotny, L. *J. Opt. A: Pure Appl. Opt.* **2009**, *11*, 114030.
(20) Bharadwaj, P.; Beams, R.; Novotny, L. *Chem. Sci.* **2011**, *2*, 136−140.
(21) Liu, N.; Tang, M. L.; Hentschel, M.; Giessen, H.; Alivisatos, A. P. *Nat. Mater.* **2011**, *10*, 631−636.
(22) Park, S. Y.; Stroud, D. *Phys. Rev. B* **2004**, *69*, 125418.
(23) Yan, J.-Y.; Zhang, W.; Duan, S.; Zhao, X.-G.; Govorov, A. O. *Phys. Rev. B* **2008**, *77*, 165301.

(24) García de Abajo, F. J.; Howie, A. *Phys. Rev. B* **2002**, *65*, 115418.
(25) Gérardy, J. M.; Ausloos, M. *Phys. Rev. B* **1982**, *25*, 4204−4229.
(26) Meier, M.; Wokaun, A. *Opt. Lett.* **1983**, *8*, 581−583.
(27) Mie, G. *Ann. Phys.* **1908**, *25*, 377−445.
(28) Bohren, C. F.; Huffman, D. *Absorption and Scattering of Light by Small Particles*; Wiley science paperback series; Wiley: New York, 1983.
(29) Tomaš, M. S. *Phys. Rev. A* **1995**, *51*, 2545−2559.
(30) Paulus, M.; Gay-Balmaz, P.; Martin, O. J. F. *Phys. Rev. E* **2000**, *62*, 5797−5807.
(31) Martin, O. J. F.; Piller, N. B. *Phys. Rev. E* **1998**, *58*, 3909−3915.
(32) Chew, W. *Waves and Fields in Inhomogeneous Media*; IEEE Press Series on Electromagnetic Waves; IEEE Press: Washington, DC, 1999.
(33) Palik, E. *Handbook of Optical Constants of Solids*; Handbook of Optical Constants of Solids v. 3; Academic Press: New York, 1998.
(34) Balanis, C. *Antenna Theory: Analysis and Design*; Harper & Row series in electrical engineering; Wiley: New York, 1982.
(35) Prodan, E.; Radloff, C.; Halas, N. J.; Nordlander, P. *Science* **2003**, *302*, 419−422.

■ NOTE ADDED AFTER ASAP PUBLICATION

This Letter was published ASAP on February 1, 2013. Equation 10 has been modified. The correct version was published on February 4, 2013.